An Optimization Model for Reliability Improvement and Cost Reduction Through EV Smart Charging

Jinping Zhao, Ali Arefi, *Senior Member*, *IEEE*, Alberto Borghetti, *Fellow*, *IEEE*, and Gerard Ledwich, *Life Fellow*, *IEEE*

***Abstract*—There is a general concern that the increasing penetration of electric vehicles (EVs) will result in higher aging failure probability of equipment and reduced network reliability. The electricity costs may also increase, due to the exacerbation of peak load led by uncontrolled EV charging. This paper proposes a linear optimization model for the assessment of the benefits of EV smart charging on both network reliability improvement and electricity cost reduction. The objective of the proposed model is the cost minimization, including the loss of load, repair costs due to aging failures, and EV charging expenses. The proposed model incorporates a piecewise linear model representation for the failure probability distributions and utilizes a machine learning approach to represent the EV charging load. Considering two different test systems (a 5-bus network and the IEEE 33-bus network), this paper compares aging failure probabilities, service unavailability, expected energy not supplied, and total costs in various scenarios with and without the implementation of EV smart charging.**

***Index Terms*—Aging failure, electric vehicle (EV), EV charging, power system reliability, expected energy not supplied, distribution network.**

I. Introduction

POWER utilities need to maintain a certain level of reliability for the electrical energy supply in distribution networks at reasonable costs [1]. Equipment aging failures are often the main reason for low reliability and power quality issues [2].

The wide use of electric vehicles (EVs) is seen as a major contribution to a sustainable global development [3]. However, the increased loading resulting from growing penetration of EVs may weaken system reliability if adequate procedures are not applied to mitigate the impact of EV charging [4]. Hence, effective reliability evaluation and reliability optimization strategies are essential for power system operators and planners in the presence of extended integration of EVs. Additionally, the exacerbation of peak period caused by random EV charging results in higher fluctuations in wholesale electricity market prices.

Reliability, defined as the probability of providing adequate electricity to the load with appropriate power quality in the planned timeframe [5], is characterized by specific indices such as system average interruption duration index (SAIDI), system average interruption frequency index (SAIFI), expected energy not supplied (EENS), loss of load probability (LOLP), customer interruption frequency (CIF), and customer interruption duration (CID) [6]-[9]. Reliability improvement methods can be classified into direct or indirect methods based on their objectives. Direct methods [10]-[12] aim to maximize the system reliability, while indirect methods [13]-[15] focus on improving network operation and performance by reducing power loss, enhancing voltage magnitude profiles, and maintaining active and reactive power balance.

From the perspective of power utility investments, reliability enhancement methods can be classified into three groups: cost-free methods (flexibility-based), non-cost-free methods (technical methods), and hybrid methods. Typical cost-free methods achieve power supply-demand balance during contingencies through load and generation scheduling, including distributed generation (DG), demand response (DR), storage units, and EV smart charging. Within this framework, the DG impact on network reliability is analyzed in [16], and a trade-off between reliability and costs is determined for considered contingencies. EV smart charging/discharging and load control algorithms are proposed in [17], [18] to alleviate peak loads and, therefore, improve system reliability. Non-cost-free methods involve costs due to the purchase and operation of specific devices, such as protections, reclosers, circuit breakers, tie lines, and distribution static synchronous compensators (DSTATCOMs) [19], [20]. Hybrid methods combine both non-cost-free and cost-free ones. For instance, in [21], the combined use of DG and cross-connections is

Manuscript received: December 19, 2022; revised: May 11, 2023; accepted: July 6, 2023. Date of CrossChecked: July 6, 2023. Date of online publication: August 16, 2023.

The authors thank Dr. Javid Maleki Delarestaghi for supporting the segment selection constraints of failure probability in Gurobi.

J. Zhao (corresponding author) and A. Arefi are with the School of Engineering and Energy, Murdoch University, Perth, Australia (e-mail: jinping.zhao@murdoch.edu.au; ali.arefi@murdoch.edu.au).

A. Borghetti is with the Department of Electrical, Electronic, and Information Engineering, University of Bologna, Bologna, 40126, Italy (e-mail: alberto.borghetti@unibo.it).

G. Ledwich is with the School of Electrical Engineering and Robotics, Queensland University of Technology, Brisbane, QLD 4000, Australia (e-mail: g.ledwich@qut.edu.au).

DOI: 10.35833/MPCE.2022.000837

proposed.

Given the significant impact on system reliability and the expected increase in EV usage, EV smart charging needs to be prioritized, as analyzed in [9], [14], [22]. Previous studies compare LOLP and EENS reliability indices for uncontrolled charging versus smart charging [23], propose time allocation strategies of home and public charging [17], quantify the maximum permissible EV load without system reliability degradation [24], [25], propose bidirectional control strategies for EV charging stations [26], or focus on optimal EV charging station allocation [27], [28]. Car parks with a large number of EVs are considered as backup energy sources to support the grid in case of feeder failure or feeder component failure [29].

Aging failure of cables is considered in [30] for transmission networks, without considering loading fluctuations and the aging process of transformers. Generally, studies on power distribution system reliability have overlooked aging failures due to insulation material degradation, assuming them to be insignificant up to now. Therefore, to the best of our knowledge, only sudden failures (repairable failure) with time-independent failure probabilities or Monte-Carlo simulations have been considered in the literature on power distribution network reliability.

The aging status of the equipment is closely related to temperature and loading conditions. Real-time dynamic thermal rating (DTR) has been shown to significantly improve system reliability in bulk power systems with accurate metering and weather data collection [31]. However, DTR is not typically applied in medium- and low-voltage distribution systems, primarily due to the inadequacy of metering systems, and it is not considered in this paper.

This paper focuses on the effects of temperature due to load fluctuations, specifically due to EV charging processes, building upon the approach introduced in our previous study [2]. Uncontrolled home charging of EVs heavily exacerbates the evening peak load [32] and reduces equipment lifespan while increasing network unavailability.

This paper proposes a reliability-based optimization procedure, with a cost minimization objective, considering customer losses resulting from node unavailability, power utility investments in replacing aged equipment, EV charging, and power losses. The developed optimization procedure considers the operational constraints of the distribution network, EV charging load, power flows, and a linear representation of the aging failure probabilities for low-voltage (LV) insulated power cables and transformers.

The main scope of this paper is to estimate the impact of EV smart charging on system reliability due to aging failure. The design of situation awareness methodologies to mitigate the effects of DG variations and sudden failures (e.g., due to extreme weather events) on system reliability is beyond the scope of this study.

The main contributions of this paper are summarized as follows.

1) The mathematical formulation of the optimization procedure is proposed for the assessment of the influence of EV smart charging on system reliability enhancement in terms of customer and power utility costs associated with aging failures of LV transformers and cables.

2) A model for accurately representing the non-linear characteristics of aging failures in transformers and cables is proposed using piecewise linear constraints.

3) A multilayer perceptron (MLP) model is proposed for the representation of EV charging load demand based on survey data.

The proposed optimization model is a mixed-integer quadratically-constrained programming (MIQCP) model, which is solved by using the Gurobi solver. The main constraints of the optimization problem include the power flow equations, the representation of EV charging, and the proposed piecewise linear model for estimating aging failures. The framework of the proposed optimization model is illustrated in Fig. 1.

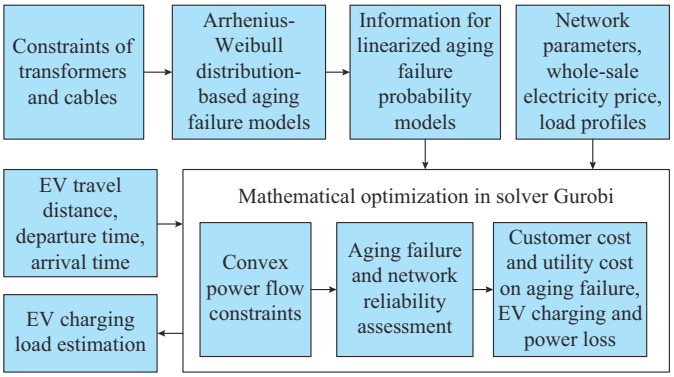

Fig. 1. Framework of proposed reliability optimization model.

This paper is organized as follows. Section II presents the formulation of the optimization procedure. Section III describes the adopted two test networks (a 5-bus network and the IEEE 33-bus network), the base load and EV charging profiles, and the selected test cases. Section IV presents and analyses the simulation results. Section V concludes this paper.

II. Formulation of Optimization Procedure

Considering the set of feeder buses N (with index i, while $i=N+1$ indicates the substation transformer (ST)) representing the customers at each bus (where customer loads, including EV charging, are aggregated), and the set of time slots T_s (with index j) representing the optimization horizon, the variables in the model are organized as:

$$\pi_1=\{E_{ij}, E_{ij}^{req}, P_{ij}^{EV}, P_{ij}^{\max} | \forall i \in N, \forall j \in T_s\} \quad (1)$$

$$\pi_2=\{P_{ij}, Q_{ij}, V_{ij}, B_{ij} | \forall i \in N, \forall j \in T_s\} \quad (2)$$

$$\pi_3=\{\lambda_{ije}^{L}, p_{ije}^{L}, p_{i}^{L} | \forall i \in N, \forall j \in T_s, \forall e \in N_s^{L}\} \quad (3)$$

$$\pi_4=\{\lambda_{ije}^{T}, p_{ije}^{T}, p_{i}^{T} | \forall i \in N+1, \forall j \in T_s, \forall e \in N_s^{T}\} \quad (4)$$

where π_1 is the set of variables for EV charging at each bus, in which E_{ij} is the energy level, E_{ij}^{req} is the required energy for being fully charged, P_{ij}^{EV} is the charging power, and $P_{ij}^{\max}$ is the maximum charging power considering the number of EVs connected to the charging stations; π_2 is the set of the power flow variables, in which P_{ij} is the active power flow,

Q_{ij} is the reactive power flow, V_{ij} is the bus voltage square magnitude, and B_{ij} is the branch current square magnitude; π_3 is the set of variables of the piecewise linear model of cable aging failure probability, in which λ_{ije}^{L} is the binary variable of the e^{th} segment, p_{ije}^{L} represents the failure probability at the e^{th} segment, and p_i^L is the failure probability of the i^{th} cable over a day; and π_4 is the set of variables of the aging failure probability piecewise linear models of distribution transformers (DTs) and the ST, in which λ_{ije}^{T} is the binary variable of the e^{th} segment, p_{ije}^{T} represents the failure probability at the e^{th} segment, and p_i^T is the failure probability of the i^{th} transformer. In this paper, subscripts/superscripts T and L are used to differentiate the parameters and variables for LV transformers and cables, respectively.

The considered time horizon is one year. To simplify the analysis, the base load demand (excluding EV charging) for the entire year is clustered as load demand for three typical days. Each day is divided into time slots of 1 hour duration. The following subsections describe the various parts of the model, the procedure for calculating the inputs, and the approach used to solve the optimization problem.

A. Objective Function

The objective function includes the customer cost (*CC*) due to aging failures, the utility cost (*UC*) for the replacement of damaged equipment, the EV charging cost (*EVC*), and the cost associated to power loss (*PLC*):

$$\min F = CC + UC + EVC + PLC \tag{5}$$

1) *CC* considers the aging failure probabilities of lines p_k^L, DTs p_i^{DT}, and ST p^{ST}. Considering the post-fault reconfiguration (e. g., circuit breaker, switches), unavailability U_i^{AF} at bus i is defined by:

$$U_i^{AF} = U_i^L + U_i^T \tag{6}$$

$$U_i^L = \sum_{k=1}^{N} RC_{ik} \cdot d_k^L p_k^L + \sum_{k=1}^{N} SC_{ik} \cdot s_k^L p_k^L \tag{7}$$

$$U_i^T = d_i^{DT} p_i^{DT} + d^{ST} p^{ST} \tag{8}$$

where RC_{ik} and SC_{ik} are the ik^{th} entries of the replacement coefficient matrix and the switching coefficient matrix, respectively [19]; d_k^L, d_i^{DT}, and d^{ST} are the durations for replacing the k^{th} line, the i^{th} DT, and the ST, respectively; and s_k^L is the switching duration of the k^{th} line.

The EENS at bus i is calculated by multiplying unavailability by the average power $\tilde{P}_i$:

$$EENS_i^{AF} = U_i^{AF} \tilde{P}_i \tag{9}$$

The value of customer reliability (VCR) and EENS estimate the customer loss due to aging failures on equipment:

$$CC(\pi_2, \pi_3, \pi_4) = \sum_{i=1}^{N} EENS_i^{AF} \cdot VCR_i \tag{10}$$

The calculation of the aggregate VCR values, considering different locational load components, is described in Section III.

2) *UC* is calculated by combining the costs for purchasing new equipment and replacing damaged ones with the aging failure probabilities for each device:

$$UC(\pi_2, \pi_3, \pi_4) = \sum_{i=1}^{N} (C_i^L p_i^L + C_i^{DT} p_i^{DT}) + C^{ST} p^{ST} \tag{11}$$

where C_i^L, C_i^{DT}, and C^{ST} are the costs for the i^{th} cable, the i^{th} DT, and the ST, respectively.

3) *EVC* for utilities is expressed as:

$$EVC(\pi_1, \pi_2) = \sum_{i=1}^{N} \sum_{j=1}^{T_s} w_j P_{ij}^{EV} \Delta t \tag{12}$$

where w_j is the wholesale electricity price at the j^{th} interval; P_{ij}^{EV} is the charging power of EVs on bus i at the j^{th} interval; and Δt is the duration of one time slot.

4) *PLC* is defined as:

$$PLC(\pi_1, \pi_2) = \sum_{i=1}^{N} \sum_{j=1}^{T_s} w_j P_{loss} \Delta t \tag{13}$$

where P_{loss} is the power loss of the whole feeder.

The components in objective function (5) are influenced by the implementation of EV smart charging. Indeed, EV smart charging reduces the power flow and loading on cables and transformers during peak hours, leading to a decrease in aging failure probabilities and an improvement in system reliability. Additionally, the adoption of EV smart charging results in a reduction in power loss and payments for EV smart charging.

B. Constraints

The constraints are related to the operational limits of the network, EV load and charging power, and the piecewise linear representation of failure probabilities for cables and transformers.

1) Probabilistic Aging Failure Constraints

Failure probabilities (p_T, p_L) of transformer and line are related to their loadings, temperatures, and the functional age (T_0). T_0 is determined by historical operations, maintenance conditions, and actual operational statuses [30]. T_s is the total number of time slots for aging failure estimation.

The real-time temperature of an equipment depends on the ambient temperature and loading conditions. References [33] and [34] show the mathematical expressions for the calculation of the temperature of cables and transformers according to the current-carrying capacity/loading ratio, thermal constants, and manufacturer data.

Higher loading increases the temperature, the relative aging speed (RAS), and the loss-of-life. The RAS is defined as the ratio between the lifespans under rated temperature (θ_r) and a specific hot-spot temperature (θ_k). RAS_k^T and RAS_k^L at the k^{th} time slot for a transformer and a cable are expressed as:

$$RAS_k^T = \exp\left(\frac{a(\theta_k^T - \theta_r^T)}{(\theta_r^T + 273)(\theta_k^T + 273)} \right) \tag{14}$$

$$RAS_k^L = 10^{\frac{b(\theta_k^L - \theta_r^L)}{(\theta_r^L + 273)(\theta_k^L + 273)}} \tag{15}$$

where a and b are the constants given by manufacturers.

Based on the Arrhenius-Weibull distribution, the cumulative distribution function (CDF) for aging failure of a transformer and a cable are expressed as:

$$CDF_T = 1 - \exp\left(-\left(\frac{T_0 + \sum RAS_k^T}{L(\theta_r^T)}\right)^{\beta_T}\right) \tag{16}$$

$$CDF_L = 1 - \exp\left(-\left(\frac{T_0 + \sum RAS_k^L}{L(\theta_r^L)}\right)^{\beta_L}\right) \tag{17}$$

where $L(\theta_r^T)$ and $L(\theta_r^L)$ are the rated lifespans of insulated transformer and cable under the rated operating temperatures θ_r^T and θ_r^L, respectively; and β_L and β_T are the shape parameters of the Arrhenius-Weibull distributions for cables and transformers, respectively.

As described in [2], based on the definition of aging failures as the conditional probability of failure occurring within a time interval after the device has operated for a specific duration, the mathematical expressions of aging failure probabilities for the transformer and cable (p_T, p_L) can be expressed as:

$$p_T = \sum_{j=1}^{T_s}\left[1 - \exp\left(\left(\frac{T_0 + \sum_{k=1}^{j-1} RAS_k^T \cdot \Delta t}{L(\theta_r^T)}\right)^{\beta_T} - \left(\frac{T_0 + \sum_{k=1}^{j} RAS_k^T \cdot \Delta t}{L(\theta_r^T)}\right)^{\beta_T}\right)\right] \tag{18}$$

$$p_L = \sum_{j=1}^{T_s}\left[1 - \exp\left(\left(\frac{T_0 + \sum_{k=1}^{j-1} RAS_k^L \cdot \Delta t}{L(\theta_r^L)}\right)^{\beta_L} - \left(\frac{T_0 + \sum_{k=1}^{j} RAS_k^L \cdot \Delta t}{L(\theta_r^L)}\right)^{\beta_L}\right)\right] \tag{19}$$

Due to the nonlinear characteristic of the aging failure probability equations, a piecewise linearization is adopted:

$$p = \begin{cases} s_1(k - k_1^{ini}) + p_1^{ini} & k_1^{ini} < k < k_2^{ini} \\ s_2(k - k_2^{ini}) + p_2^{ini} & k_2^{ini} < k < k_3^{ini} \\ \vdots & \vdots \\ s_{N_s-1}(k - k_{N_s-1}^{ini}) + p_{N_s-1}^{ini} & k_{N_s-1}^{ini} < k < k_{N_s}^{ini} \end{cases} \tag{20}$$

where s_e is the slop of the e^{th} segment, and $e = 1, 2, \ldots, N_s$; and k_e^{ini} and p_e^{ini} are the initial location of the breakpoint and the initial failure probability of the e^{th} segment, respectively. The ending location of the breakpoint of the $(e-1)^{\text{th}}$ segment k_{e-1}^{end} is the equal to the initial location of the breakpoint of the e^{th} segment k_e^{ini}. The so-called big-M formulation is adopted for the representation of the aging failure probabilities for cables and transformers:

$$\sum_{e=1}^{N_s} \lambda_{ije} \le 1 \tag{21}$$

$$k_{e_0}^{end} - k_{ij} \le M \sum_{e=1}^{e_0} \lambda_{ije} \quad \forall e_0 \in \{1, 2, \ldots, N_s\} \tag{22}$$

$$k_{e_0}^{end} - k_{ij} \ge -M \sum_{e=1}^{e_0} \lambda_{ije} \quad \forall e_0 \in \{1, 2, \ldots, N_s\} \tag{23}$$

$$p_{ije} \le s_e(k_{ij} - \lambda_{ije} k_e^{ini}) + p_e^{ini} \tag{24}$$

$$p_{ije} \ge s_e(k_{ij} - \lambda_{ije} k_e^{ini}) + p_e^{ini} - M(1 - \lambda_{ije}) \tag{25}$$

$$p_{ije} \le M\lambda_{ije} \tag{26}$$

$$p_{ije} \ge 0 \tag{27}$$

$$p_i = \sum_{j=1}^{T_s}\sum_{e=1}^{N_s} p_{ije} \tag{28}$$

where λ_{ije} is the binary variable; p_{ije} is the failure probability of the e^{th} segment on the i^{th} equipment at the j^{th} interval; p_i is the aging failure probability at the i^{th} equipment; M is a big number (e.g., 1000); and k_{ij} is the actual load in per unit for the i^{th} transformer and temperature for the i^{th} cable at the j^{th} interval.

Constraints (21)-(23) determine the specific segment utilized according to the value of k_{ij}. Constraints (24)-(27) define the failure probability at each segment. Assuming $\lambda_{ije} = 0$, to meet the constraints (26) and (27), $p_{ije} = 0$; otherwise, constraints (24) and (25) are equivalent to:

$$p_{ije} = s_e(k_{ij} - \lambda_{ije} k_e^{ini}) + p_e^{ini} \tag{29}$$

The total failure probability p_i is defined in (28) by the summation of all the failure probability at each segment during all intervals. The accuracy of the linearization depends on the number of segments. A large number of segments lead to high accuracy but increase the solution time. The PWLF Python library [35] is used to find the optimal breakpoint locations for all segments by employing least squares fitting, considering the specified number of line segments.

The aging failure probabilities of transformers when load varies from 0 p.u. to 2.0 p.u. by 0.001 are calculated using (14). These values are the inputs of the PWLF library based procedure that finds the optimal breakpoints ($k_e^{T,ini}$, $k_e^{T,end}$), slopes (s^T), and initial failure probability ($p^{T,ini}$) for each segment. The piecewise linearization method demonstrates good performance when the number of segments is set to be 10, as observed from the comparison of failure probabilities using the linearized equations and the original model. Figure 2 illustrates the comparison between the original and linearized data for aging failure probability on a transformer. The sum-of-square error for this comparison is calculated to be 1.91×10^{-10}.

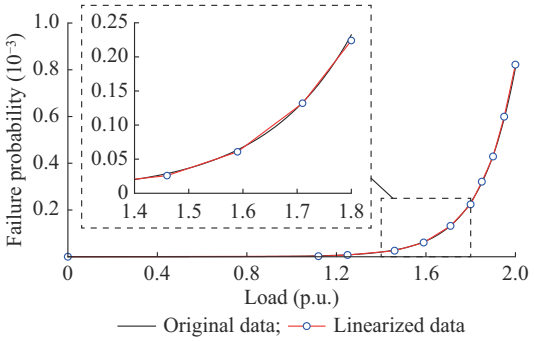

Fig. 2. Original and linearized data for aging failure probability on transformer.

A similar procedure is adopted to linearize the aging failure probability of a cable based on the temperature. Following the approach described in [33], the temperature is influenced by the branch current obtained from power flow calculation and its specifications, such as square current-carry capacity (B_Z), ambient reference temperature (θ_0), ambient tem-

perature (θ_a), and thermal time constant (τ), as shown in (30).

$$k_j^L=(\theta_r^L-\theta_0)\frac{B_j}{B_Z}\left(1-\mathrm{e}^{\frac{-\Delta t}{\tau}}\right)+(k_{j-1}^L-\theta_0)\frac{B_{j-1}}{B_Z}\mathrm{e}^{\frac{-\Delta t}{\tau}}+\theta_a \quad (30)$$

The input is the temperature (varied from 0 ℃ to 100 ℃) and the output is the aging failure probability for the piecewise linearization. Aging failure probabilities of cables are obtained using (19). Breakpoints ($k_e^{L,ini}, k_e^{L,end}$), slope (s^L), and initial failure probability ($p^{L,ini}$) are determined using the PWLF library [36]. The comparison between the original and linearized data for aging failure probability on cable is shown in Fig. 3 with 10 segments. The sum-of-square error is 8.42×10^{-12}.

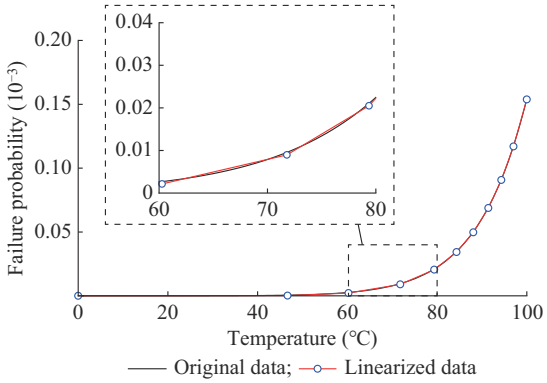

Fig. 3. Original and linearized data for aging failure probability on cable.

Table I shows the piecewise linearization information of each segment for the calculation of aging failure probabilities assuming the loss of life of historical operation are 170000 and 165000 hours for transformers and cables, respectively. The initial load and temperatures ($k^{T,ini}, k^{L,ini}$) of the e^{th} segment are the ending load and temperatures ($k^{T,end}, k^{L,end}$) of the $(e-1)^{\text{th}}$ segment. The R^2 values are 99.995% and 99.997%, and the standard errors are in the interval $[2.09\times10^{-7}, 4.16\times10^{-5}]$ and $[2.35\times10^{-7}, 4.71\times10^{-5}]$ for each segment of aging failure probabilities of transformers and cables, respectively.

TABLE I
PIECEWISE LINEARIZATION INFORMATION FOR TRANSFORMERS AND CABLES

Segment No.	Transformer			Cable		
	$p^{T,ini}$	s^T	$k^{T,ini}$ (p.u.)	$p^{L,ini}$	s^L	$k^{L,ini}$ (℃)
1	9.07×10^{-9}	2.61×10^{-6}	0	1.40×10^{-9}	2.86×10^{-9}	0
2	2.20×10^{-6}	4.02×10^{-5}	1.12	1.36×10^{-7}	1.47×10^{-7}	46.67
3	7.60×10^{-6}	9.01×10^{-5}	1.25	2.14×10^{-6}	5.93×10^{-7}	60.27
4	2.59×10^{-5}	2.59×10^{-4}	1.46	8.97×10^{-6}	1.55×10^{-6}	71.79
5	6.08×10^{-5}	5.77×10^{-4}	1.59	2.05×10^{-5}	2.78×10^{-6}	79.37
6	1.32×10^{-4}	1.12×10^{-3}	1.71	3.43×10^{-5}	4.13×10^{-6}	84.34
7	2.24×10^{-4}	1.71×10^{-3}	1.80	4.97×10^{-5}	5.70×10^{-6}	88.07
8	3.21×10^{-4}	2.32×10^{-3}	1.85	6.88×10^{-5}	7.57×10^{-6}	91.43
9	4.29×10^{-4}	3.16×10^{-3}	1.90	9.07×10^{-5}	9.74×10^{-6}	94.33
10	5.99×10^{-4}	4.46×10^{-3}	1.95	1.17×10^{-4}	1.24×10^{-5}	97.03

The parameters of the piecewise linear model of cable aging failure probability refer to a generic insulated LV power cable. Obtaining specific information on the type of cables installed in the distribution network is crucial for developing accurate models that can be effectively used in a specific study.

2) EV Load Prediction and Constraints

A multi-layer perceptron (MLP) model predicts the travel mileages of EV in the test system. The typical MLP model is structured by an input layer, multiple hidden layers, and an output layer. The mathematical relationship between input layer ($\boldsymbol{X}$) and output layer ($\boldsymbol{O}$) of an MLP with one hidden layer ($\boldsymbol{H}$) is expressed as [36]:

$$\boldsymbol{H}=f(\boldsymbol{\mu}_h\boldsymbol{X}^{\mathrm{T}}+\boldsymbol{\sigma}_h) \quad (31)$$

$$\boldsymbol{O}=g(\boldsymbol{\mu}_o\boldsymbol{H}^{\mathrm{T}}+\boldsymbol{\sigma}_o) \quad (32)$$

where $\boldsymbol{\mu}_h$, $\boldsymbol{\sigma}_h$, and $f(\cdot)$ are the weights, biases, and activation function of hidden layer, respectively; and $\boldsymbol{\mu}_o$, $\boldsymbol{\sigma}_o$, and $g(\cdot)$ are the weights, biases, and activation function of output layer, respectively.

The open data of 2017 National Household Travel Survey (NHTS) [37] are utilized to study the driving behavior of EV owners and train the MLP model. To ensure a better representation of practical experience, EVs with travel distance larger than 250 miles have been removed from the original dataset. The modified NHTS dataset is then divided into two parts: 80% for training the MLP model and 20% for testing the evaluation accuracy. The MLP model is trained using the Scikit-learn Python library, with a configuration of 100 epochs and a batch size of 5. The accuracy evaluation metrics used include correlation coefficient R^2, mean squared error (MSE), and mean absolute error (MAE). Based on the evaluation results, the MLP architecture with 3 hidden layers and 50 nodes demonstrates the best performance, achieving approximately 1.0000 for R^2, 0.0035 for MSE, and 0.0124 for MAE.

The probabilistic distribution functions of vehicle departure time (f_{dep}) and arrival time (f_{arr}) have been modelled as normal distributions:

$$f_{dep}=\frac{1}{3.04\sqrt{2\pi}}\mathrm{e}^{-\frac{1}{2}[(t-9.21)/3.04]^2} \quad 0<t<24 \quad (33)$$

$$f_{arr}=\frac{1}{3.52\sqrt{2\pi}}\mathrm{e}^{-\frac{1}{2}[(t-16.43)/3.52]^2} \quad 0<t<24 \quad (34)$$

These normal distributions are used to generate the EV arrival time vector ($\boldsymbol{T}_i^{arr}$) and departure time vector ($\boldsymbol{T}_i^{dep}$), given the number of EVs in the test system. The time range for optimizing the aggregated EV charging load is between the earliest arrival time and earliest departure time for simplicity, as shown in Fig. 4. Since the time horizon for an interval is 1 hour, the floor and ceiling functions are utilized to assign the arrival time and departure time of all EVs to the corresponding intervals.

The newly generated vectors of $\boldsymbol{T}_i^{arr}$ and $\boldsymbol{T}_i^{dep}$ are the inputs of the pre-trained MLP model to predict the EV travel mileage vector ($\boldsymbol{d}^e$).

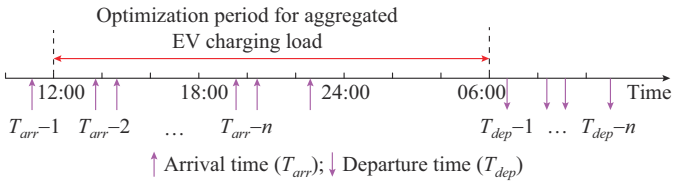

Fig. 4. Time range for optimizing aggregated EV charging load.

Combining the travel mileage and the EV battery data (i.e., rated charging power and capacity), the state-of-charge (SoC) level (SoC_{il}), the initial stored energy (E_{il}^{ini}), and the required energy ($E_{il}^{req,ini}$) of the l^{th} EV connected to the i^{th} bus are calculated by (35)-(37), respectively.

$$SoC_{il}=\frac{D_{il}^{r}-\omega_{il}d_{il}^{e}}{D_{il}^{r}} \tag{35}$$

$$E_{il}^{ini}=SoC_{il}\cdot C_{il}^{r} \tag{36}$$

$$E_{il}^{req,ini}=(1-SoC_{il})C_{il}^{r} \tag{37}$$

where D_{il}^{r}, ω_{il}, d_{il}^{e}, and C_{il}^{r} are the rated travel mileage, type (e.g., full electric or hybrid), expected travel mileage, and rated capacity of the l^{th} EV on the i^{th} bus, respectively. Before being used in the optimization algorithm, these parameters need to be categorized in a time sequence. The EV penetration (φ) is defined as the ratio of the total number of EVs to the total number of houses.

To generate the optimized EV load at each bus, the following constraints (38)-(43) are implemented. Constraints (38) and (39) define the limit of charging power. The maximum charging power of bus i at the j^{th} interval $P_{ij}^{\max}$ is furtherly confined by (43). According to constraint (40), all EVs need to be fully charged before any journey on the next day. Constraints (41) and (42) are utilized to calculate the energy required and energy stored by EVs on the i^{th} bus at the j^{th} interval, respectively.

$$P_{ij}^{EV}\geq 0 \tag{38}$$

$$\eta_{ij}^{a}P_{ij}^{EV}\leq P_{ij}^{\max} \tag{39}$$

$$\sum_{j=1}^{T_s}E_{ij}^{req,ini}=\sum_{j=1}^{T_s}\eta_{ij}^{a}P_{ij}^{EV}\Delta t \tag{40}$$

$$E_{ij}^{req}=E_{ij-1}^{req}+E_{ij}^{req,ini}-\eta_{ij}^{a}P_{ij}^{EV}\Delta t \tag{41}$$

$$E_{ij}=E_{ij-1}+E_{ij}^{ini}+\eta_{ij}^{a}P_{ij}^{EV}\Delta t \tag{42}$$

$$P_{ij}^{\max}=\begin{cases}P_{ij}^{c,r} & E_{ij}^{req}\geq P_{ij}^{c,r}\Delta t\\ E_{ij}^{req}/\Delta t & E_{ij}^{req}<P_{ij}^{c,r}\Delta t\end{cases} \tag{43}$$

where η_{ij}^{a} is the average charging efficiency; $P_{ij}^{r,c}$ is the rated charging power of EV on the i^{th} bus at the j^{th} interval; and $E_{ij}^{req,ini}$ is the initial required energy by the EVs at bus i after they arrive at their respective homes.

3) Power Flow Constraints

The power flow calculation in the optimization model is based on the DistFlow model introduced in [38], [39] for radial networks. The power flow line model is illustrated in Fig. 5, representing a branch of the feeder with the load located at the receiving end. Several assumptions are made: the voltage at the substation (bus 0) is fixed and equal to 1 p.u., the network has a radial configuration so that the number of buses is equal to that of branches (the branches are identified by the respective numbers of the receiving-end buses), the network is balanced, the single line representation is adopted, and the line charging currents are neglected.

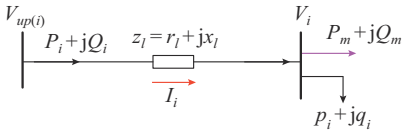

Fig. 5. Illustration of power flow line model.

The formulas of the model are expressed as:

$$P_i=p_i+r_iB_i+\sum_k A_{ik}P_k \tag{44}$$

$$Q_i=q_i+xB_i+\sum_k A_{ik}Q_k \tag{45}$$

$$V_i=V_{up(i)}-2(r_iP_i+x_iQ_i)+(r_i^2+x_i^2)B_i \tag{46}$$

$$P_i^2+Q_i^2-V_{up(i)}B_i\leq 0 \tag{47}$$

$$V_i\geq 0 \tag{48}$$

$$B_i\geq 0 \tag{49}$$

$$V_i^{\min}\leq V_i\leq V_i^{\max} \tag{50}$$

$$B_i\leq B_i^{\max} \tag{51}$$

$$P_{loss}=\sum_{i=1}^{N}r_iB_i \tag{52}$$

where P_i, Q_i, V_i, and B_i are the active power flow at the sending end of the branch, reactive power flow at the sending end of the branch, the bus voltage square magnitude, and the branch current square magnitude, respectively; $V_{up(i)}$ is the square voltage at the sending bus of the i^{th} branch; P_m and Q_m are the total active power and reactive power of branch/branches connected by the i^{th} bus directly, respectively, which are calculated by the oriented graph matrix $\boldsymbol{A}$; A_{ik} is the ik^{th} entry of $\boldsymbol{A}$, it is equal to 1 when the i^{th} bus is the sending bus of the k^{th} branch, 0 for otherwise; p_i and q_i are the active power and reactive power drawn from the i^{th} bus, respectively; r_i and x_i are the resistance and reactance of the i^{th} branch, respectively; $V_i^{\min}$ and $V_i^{\max}$ are the lower bound and upper bound for square voltage (e.g., 0.9025 p.u. and 1.1025 p.u.), respectively; and $B_i^{\max}$ is the upper bound for square current at the i^{th} branch (e.g., 2 times of square of rated current).

Constraints (44)-(49) are the power flow formulas [40]. Constraints (50) and (51) limit the voltage and current, respectively. Constraint (52) calculates the power loss of network.

C. Solution Approach

The flowchart of the solution approach is illustrated by Fig. 6. The MIQCP model incorporates various components, including decision variables, objective function tailored to the simulation scenario, constraints for equipment aging failure probabilities, EV charging representation, power flow model, and current and voltage limits. The proposed MIQCP

model is solved by using the Gurobi 9.1 solver. All the input parameters of the test cases are described in Section III.

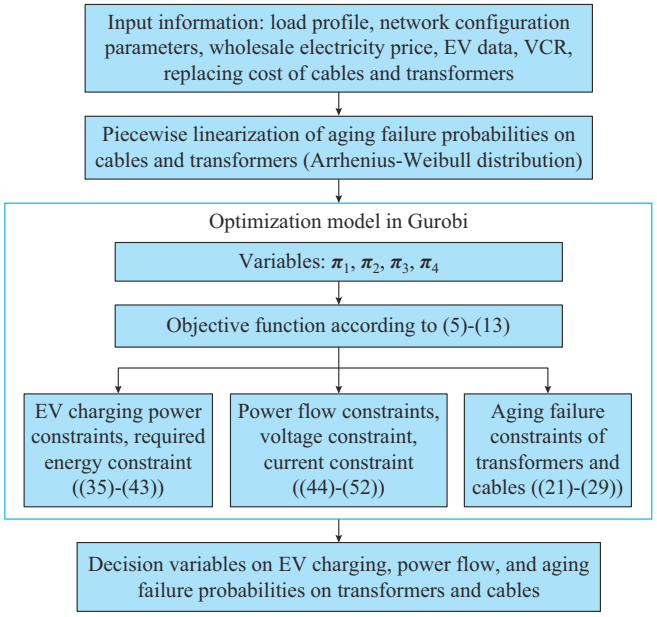

Fig. 6. Flowchart of solution approach.

III. Simulation Cases

A. Test Networks

The proposed procedure is applied to two different test networks: a 5-bus network and the IEEE 33-bus network.

The 5-bus network, shown in Fig. 7, is used to illustrate the main characteristics and feasibility of the proposed method. Bus 0 (B0) is the slack bus with fixed voltage (1.0 p.u.) at the primary side of the ST. DTs (DT1-DT5) are connected by all the buses, and all the branches 1-5 (L1-L5) are named after their receiving-end bus numbers (B1-B5). A circuit breaker is positioned at branch 1, a manual switch is installed at branch 3, and two fuses are located at branches 4 and 5.

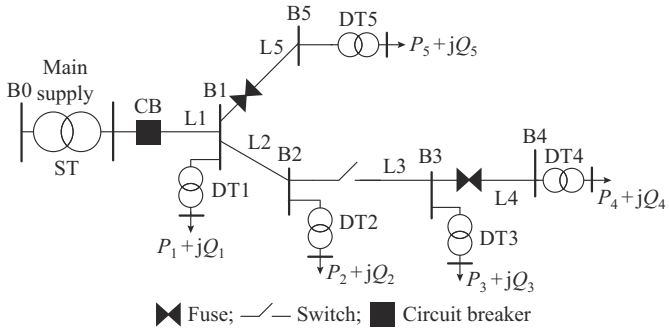

Fig. 7. Configuration of 5-bus network [19].

Table II shows the bus data including number of customers, rated load active power, DT capacity at 1.0 power factor, and weighted VCR values at each bus [28]. Parameters of transformers and cables are adapted from [34], [41]. The nominal lifespans for transformers and cables are 180000 and 175200 hours for the rated temperatures of 110 ℃ and 80 ℃, respectively. The replacement time of the substation transformer (r^{ST}), DTs (r^{DT}), lines (r^{L}), and the tripping time (s^{L}) of protecting devices is 30 hours, 20 hours, 20 hours, and 0.5 hour, respectively. The current-carrying capacities at the reference ambient temperatures (θ_{a0}) for branches 1-5 are 300 A, 150 A, 100 A, 50 A, and 50 A, respectively. Table III shows the power utility costs for replacing branches and transformers, taking the equipment cost and installation cost into consideration [20].

TABLE II
Bus Data

Bus No.	Number of customers	Rated load (kW)	Transformer capacity (kW)	VCR (AUD/kWh)
1	50	240	240	37.21
2	40	200	240	36.38
3	60	240	240	38.46
4	30	120	240	25.95
5	30	120	240	25.95

TABLE III
Replacement Cost for Branches and Transformers

No.	Replacement cost (kAUD)		
	Branch	DT	ST
1	66	70	200
2	132	70	-
3	98	76	-
4	102	70	-
5	186	70	-

To further assess the applicability of the proposed optimization procedure, IEEE 33-bus network [42], already used in [43], is employed. The network has one substation transformer of 5 MVA, 32 DTs, and 32 branches numbered by the ending bus of each branch. The rated power of the load at the buses are 100 kW (bus 1), 90 kW (buses 2, 17-22), 120 kW (buses 3, 13, 28, 29, 31), 60 kW (buses 4, 5, 8, 9, 11, 12, 14-16, 25-27), 100 kW (buses 6, 7), 40 kW (bus 10), 210 kW (buses 23, 24), 150 kW (bus 30), 80 kW (bus 32), with power factor of 0.895. The current-carrying capacities at the reference ambient temperature are 300 A, 200 A, 100 A, and 50 A for branch 1, branch 2, branches 3-5, and branches 6-32, respectively.

The losses of life due to historical operation for all the transformers and cables are equal to 170000 hours and 165000 hours, respectively, for both test networks. The piecewise linearization of Table I is used to estimate the aging failure for transformers and cables. The base load is generated by multiplying the nominal load with different load profiles described in the next subsection. The EV charging load is provided by the implemented MLP model.

B. Base Load, Electricity Price, and EV Charging Load

Residential load forecasting plays an important role in short-term operation of distribution system and the application of demand response techniques [44]. As this paper focuses on evaluating the effect from smart EV charging on

system reliability due to aging failure in a long-term (i.e., 1 year), clustered load profiles with corresponding probabilities from [45] are utilized to represent the base load. Considering the focus of the paper and for the sake of simplicity, we assume that all the EVs are of the same type (full electric), disregarding various factors such as low-carbon awareness and governmental subsidies that may influence the penetration and types of EVs in reality.

Figure 8 shows the clustered load profile (3 typical days, denoted as clusters 1-3) without EV integration for a year. The probabilities of clusters 1-3 are 31%, 17%, and 52%, respectively. The corresponding wholesale electricity prices for each typical day are also shown in Fig. 8.

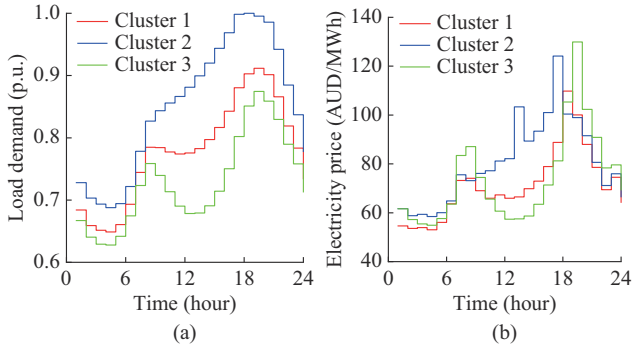

Fig. 8. Clustered load profile without EV and wholesale electricity prices. (a) Load profile. (b) Electricity price.

The rated travel mileage is 120. The rated capacity is 40 kWh. The maximum uncontrolled charging power is 10 kW. Assuming a EV penetration of 200% (i.e., every house has two EVs) in the test system, the departure time and arrival time are input to the pre-trained MLP model to predict the travel mileage of each EV. Then, SoC, the energy left and needed of each EV can be calculated by (31)-(33). After collecting those data, the aggregated information of each bus is summarized.

Figure 9 shows the EV charging load profiles with uncontrolled charging mode at buses 1-5 with a EV penetration of 200%. Uncontrolled charging starts when customers arrive their homes. Load demand from EV charging is not only dependent on the number of EVs but related to the travel distance. Therefore, even if bus 4 and bus 5 are feeding users with the same number of EVs, the average EV charging load is higher at bus 4 compared with that at bus 5 due to longer travel distances.

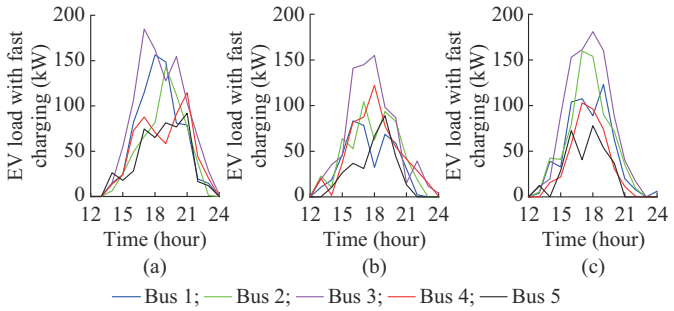

Fig. 9. EV charging load profiles ($\rho = 200\%$) with uncontrolled charging mode. (a) Cluster 1. (b) Cluster 2. (c) Cluster 3.

C. Test Cases

Three cases are considered as follows.

Case 1: the costs related to aging failure and power utilities are calculated for the uncontrolled EV charging mode, without any optimization.

Case 2: the effects of the optimization are analyzed with the objective of minimizing the sum of charging costs and power loss costs, represented by $EVC + PLC$ in (5).

Case 3: the effects of the optimization are analyzed by considering all the components of objective function (5).

IV. Simulation Results and Analysis

This section first compares the results of integrated load, aging failure probabilities of transformers and cables, customer loss due to aging failures, utility cost for managing aging failure, and utility payment on the wholesale market for EV charging load and power loss for the 5-bus network. Then, the simulation results on the IEEE 33-bus network are presented to illustrate the feasibility and effectiveness of the proposed optimization procedures.

A. Simulation Results on 5-bus Network

1) Total Load Including EV Charging for Different Cases

The simulation results of total loads including optimized EV charging demands with different objective functions are compared with uncontrolled charging for 3 clusters, respectively, as shown in Figs. 10-15.

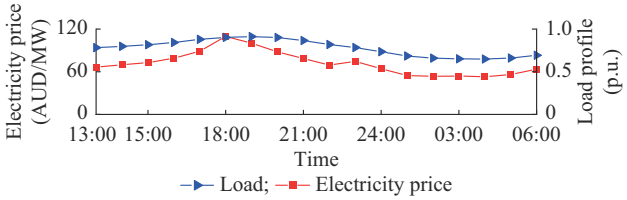

Fig. 10. Base load and electricity price for cluster 1 from 13:00 to 06:00.

Figures 10, 12, and 14 show the base load and electricity prices for clusters 1-3 from 13:00 to 06:00 next day without EV charging load. Typically, peak load occurs from 17:00 to 21:00 with higher electricity price. Figures 11, 13, and 15 show the total loads including EV charging demands at ST and each bus of different cases for clusters 1-3. For case 1 (uncontrolled EV charging mode), the load peak exacerbates when electricity price is high. For case 2 (minimization of utility cost to feed EV load and power loss), the EV charging load is shifted to the period when electricity price is low. For case 3 (minimization of the total costs including reliability), the load demands at ST and each bus have the minimum fluctuations.

2) Aging Failure Probability

This subsection presents aging failure probabilities of cables and transformers for the considered 3 cases in a year. As aging failure probability is affected by temperature and power flow, all the cables and transformers have the highest aging failures due to high aging speeds at peak hours for case 1, as shown in Table IV.

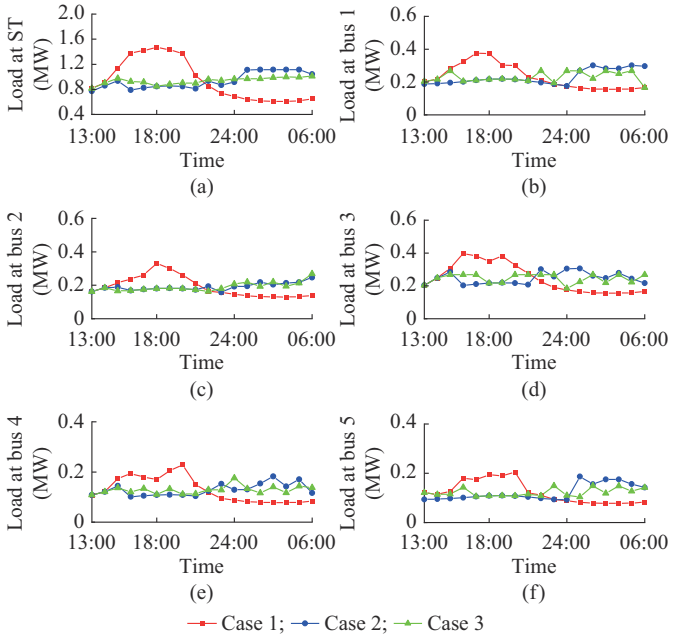

Fig. 11. Comparison of total loads including EV charging demand at ST and buses 1-5 for cases 1-3 of cluster 1. (a) At ST. (b) At bus 1. (c) At bus 2. (d) At bus 3. (e) At bus 4. (f) At bus 5.

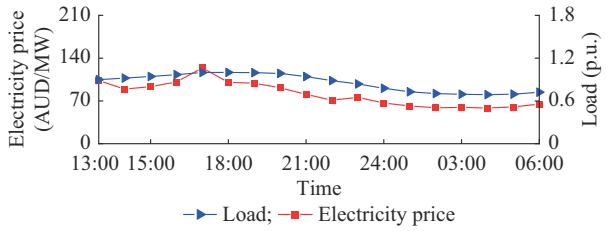

Fig. 12. Base load and electricity price for cluster 2 from 13:00 to 06:00.

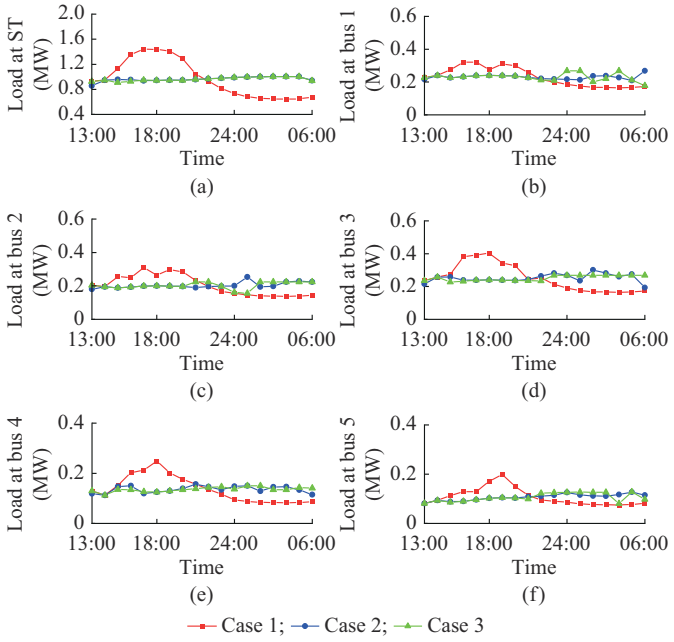

Fig. 13. Comparison of total loads including EV charging demand at ST and buses 1-5 for cases 1-3 of cluster 2. (a) At ST. (b) At bus 1. (c) At bus 2. (d) At bus 3. (e) At bus 4. (f) At bus 5.

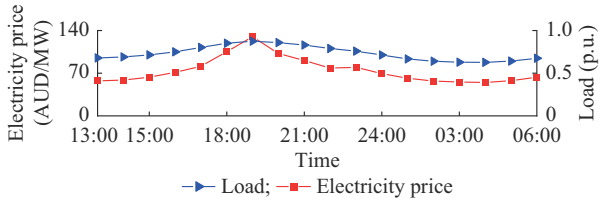

Fig. 14. Base load and electricity price for cluster 3 from 13:00 to 06:00.

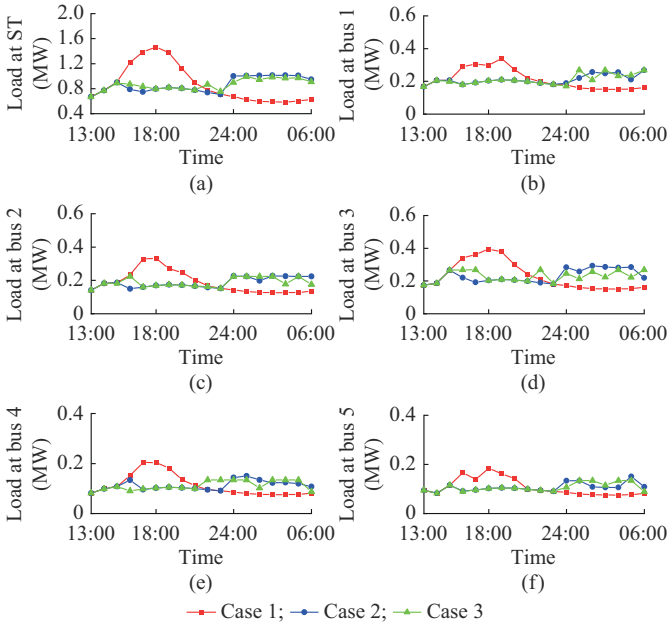

Fig. 15. Comparison of total load including EV charging demand at ST and buses 1-5 for cases 1-3 of cluster 3. (a) At ST. (b) At bus 1. (c) At bus 2. (d) At bus 3. (e) At bus 4. (f) At bus 5.

TABLE IV
AGING FAILURE PROBABILITIES OF CABLES AND TRANSFORMERS

Item	Aging failure probability (%)		
	Case 1	Case 2	Case 3
Cable 1	100.000	6.890	7.307
Cable 2	63.690	7.094	2.145
Cable 3	5.762	0.338	0.410
Cable 4	0.075	0.072	0.074
Cable 5	0.070	0.071	0.073
DT1	3.747	1.067	0.905
DT2	6.294	1.552	0.938
DT3	10.030	2.163	0.979
DT4	16.510	1.733	0.956
DT5	4.483	1.447	0.911
ST	3.089	1.401	1.348

The aging failure probability of cable 1 is 100%, indicating the termination of its life within one year when the operation loss of life for cable 1 is 165000 hours respect to its total lifespan of 180000 hours. For cable 2, the aging failure probability is higher than 50% in case 1. Cables 4 and 5 show similar aging failure probabilities for case 2 and case 3 since the minimization of the electricity payments reduces the loading fluctuations.

Similarly, the aging failure probabilities of ST and DTs are reduced in cases 2 and 3 compared with case 1. As expected, all transformers have the lowest failure probability in Case 3, which also depends on the transformer capacity. To better illustrate the impact of EV smart charging on the equipment aging failure, Fig. 16 compares the aging failure probabilities without (case 1) and with EV smart charging (cases 2 and 3) according to the data in Table IV.

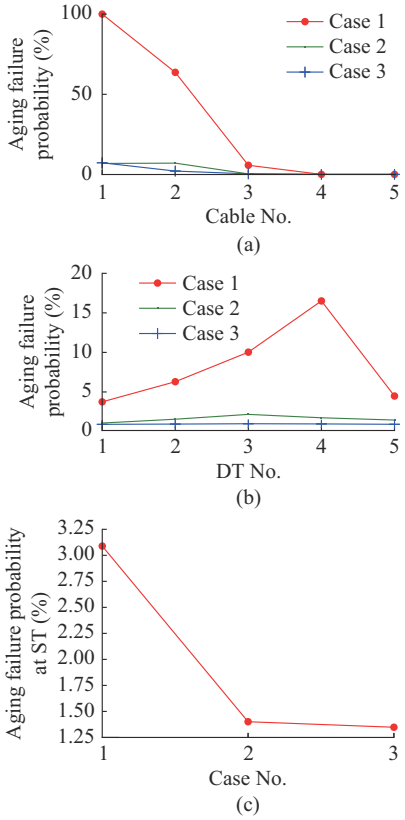

Fig. 16. Comparison of aging failure probabilities without/with EV smart charging in 5-bus network. (a) Cable. (b) DT. (c) ST.

3) *Reliability Indices and Total Cost*

Tables V and VI show the probabilistic network reliability indices including bus unavailability and EENS for the considered three cases in a year. For case 1, the highest unavailability is at bus 5 followed by bus 2 and bus 1. The maximum EENS occurs at bus 1. Compared to case 1 with average unavailability of 23.024 hours, the average unavailabilities in cases 2 and 3 are 2.383 hours and 1.785 hours, respectively. Moreover, the average EENSs are 2850.7, 298.4, and 228.11 kWh in cases 1-3, respectively. The comparison of node unavailability and EENS without (case 1) and with EV smart charging (cases 2 and 3) is also shown in Fig. 17.

TABLE V
BUS UNAVAILABILITY FOR CASES 1-3

Case	Unavailability (hour)					
	Bus 1	Bus 2	Bus 3	Bus 4	Bus 5	Average
Case 1	34.440	34.950	4.904	6.215	34.610	23.020
Case 2	3.481	3.443	0.813	0.765	3.411	2.383
Case 3	2.478	2.484	0.730	0.740	2.494	1.785

TABLE VI
EENS FOR CASES 1-3

Case	EENS (kWh)					
	Bus 1	Bus 2	Bus 3	Bus 4	Bus 5	Average
Case 1	5291.20	4295.60	903.98	572.860	3189.60	2850.70
Case 2	533.13	421.73	151.95	71.824	313.36	298.40
Case 3	389.96	312.80	132.20	68.130	235.46	228.11

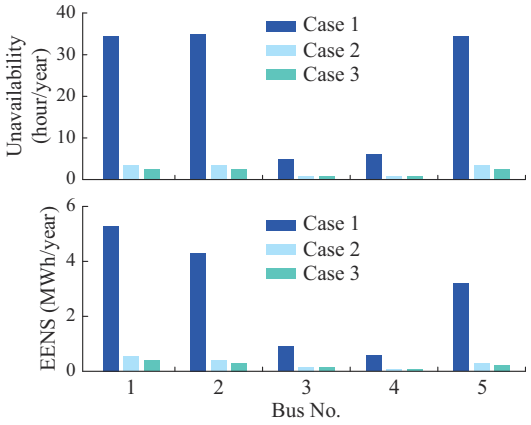

Fig. 17. Comparison of unavailability and EENS without and with EV smart charging in 5-bus network.

The values of *EVC*, *PLC*, *UC*, and *CC* in a year are presented in Table VII and Fig. 18. The total costs are 797.71, 138.2, and 129.38 kAUD for cases 1-3, respectively. The total cost declines significantly with the use of smart charging algorithms. Compared with case 2, in case 3, *EVC* and *CC* increase, whilst *UC* and *CC* decrease. Figure 16 shows the values of total cost function F defined in (5) in different cases.

TABLE VII
COSTS FOR 5-BUS NETWORK

Case	Cost (kAUD)				
	EVC	*PLC*	*UC*	*CC*	Total
Case 1	107.97	12.71	191.46	458.57	797.71
Case 2	70.67	8.64	16.79	42.11	138.21
Case 3	73.45	8.70	13.63	33.60	129.38

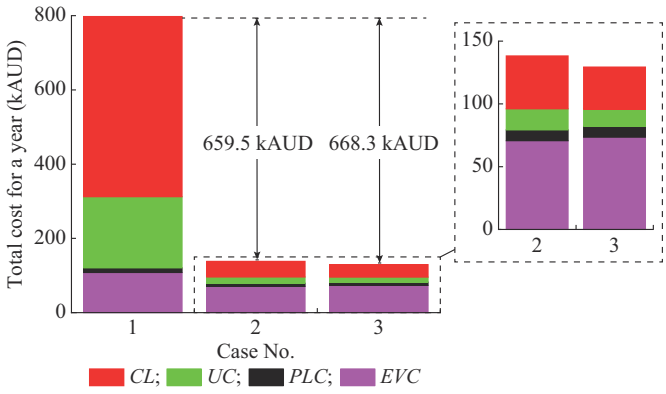

Fig. 18. Total cost without and with optimization for 5-bus network.

With EV charging load optimization, there is a yearly cost reduction of 659.5 kAUD (case 2) and 668.3 kAUD (case 3) with respect to the fast-charging condition (case 1).

B. Simulation Result on IEEE 33-Bus Network

The base load, EV charging load profile, and VCR are the same as those adopted for the 5-bus network. Aging failure probabilities of cables and transformers for the considered 3 cases based on the proposed model are calculated by applying the procedures presented in Section II. Aging failure probability for ST is reduced from 3.22% (case 1) to 1.26% (case 2) and 1.10% (case 3). The highest aging failure probability reduction is the one of DT23: from 29.4% (case 1) to 2.04% (case 2) and 1.50% (case 3) with EV smart charging. The aging failure on cable 1 reduces from 9.88% to 0.07% with EV charging optimization.

Figure 19 shows the aging failure probabilities for the ST, six selected cables (Nos. 1, 2, 12, 16, 24, 30), and the DTs (Nos. 9, 12, 23, 24, 29, 31) without and with EV smart charging in IEEE 33-bus network. As expected, compared with cases 2 and 3, the aging failure probabilities on cables and transformers are higher due to uncontrolled EV charging in case 1.

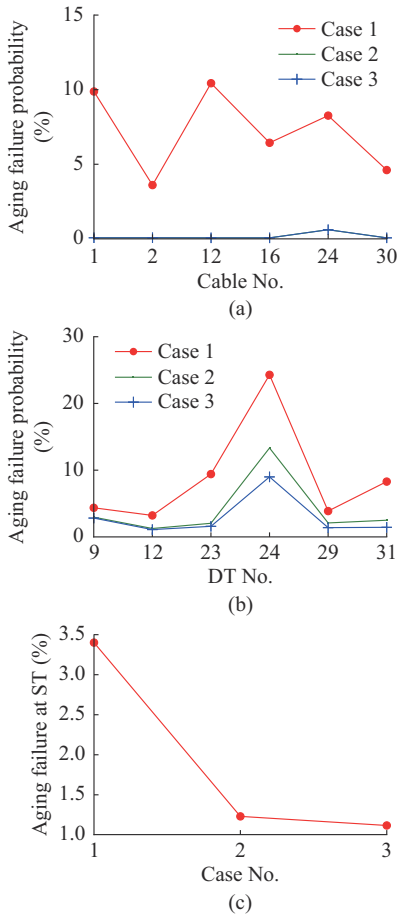

Fig. 19. Aging failure probabilities of cables and transformers without/with EV smart charging in IEEE 33-bus network. (a) Cable. (b) DT. (c) ST.

Similarly, the unavailability and EENS for a year at buses 9, 12, 23, 24, 29, and 31 without and with EV smart charging in IEEE 33-bus network are presented in Fig. 20. With lower aging failure probability for cases 2 and 3 with EV smart charging, as expected, the unavailability and EENS are lower compared with the results in case 1.

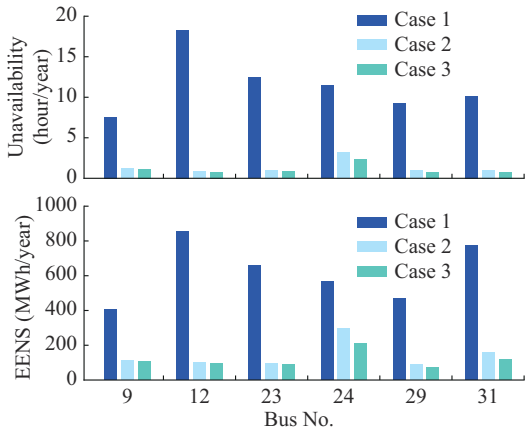

Fig. 20. Comparison of unavailability and EENS on selected buses without/with EV smart charging in IEEE 33-bus network.

The yearly cost related to EV charging, power loss, and reliability cost due to aging failure is shown in Table VIII and Fig. 21 for the test cases. Compared with the cost of 1160.2 kAUD for case 1, the total cost is reduced to 743.67 kAUD and 692.42 kAUD for cases 2 and 3, respectively. As expected, the insulation aging on transformers and cables are improved with EV smart charging, thus leading to higher reliability and lower cost.

TABLE VIII
COSTS FOR IEEE 33-BUS NETWORK

Case	Cost (kAUD)				
	EVC	*PLC*	*UC*	*CC*	Total
Case 1	668.81	43.93	89.51	357.96	1160.20
Case 2	549.54	18.21	39.73	136.19	743.67
Case 3	550.25	19.62	25.24	97.31	692.42

The *EVC*, *PLC*, *UC*, and *CC* values for the IEEE 33-bus network are higher due to the complexity of network, larger number of EV integration, and higher power losses on the branches compared with the simulation results of the 5-bus network. However, as illustrated in Fig. 19, the total cost reductions are 416.5 kAUD and 467.8 kAUD by EV smart charging for case 2 and case 3, respectively. These smaller values with respect to those relevant to the 5-bus network are justified by the lower base load and less thermal effect.

V. CONCLUSION

This paper presents an optimization procedure based on an MIQCP model including the linearized aging failure models for transformers and cables, EV charging constraints, and power flow calculation. The procedure can assess network reliability improvement and utility cost reduction obtained by the optimization of EV charging load.

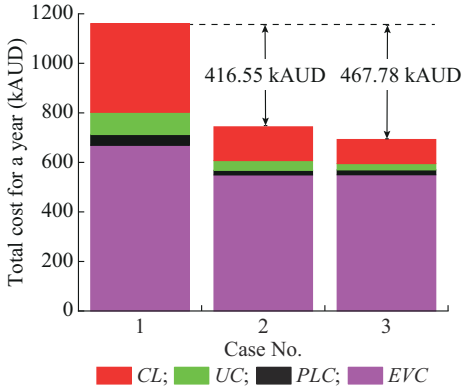

Fig. 21. Total cost without and with optimization for IEEE 33-bus network.

The application of the procedure to two different test networks (a 5-bus network and the IEEE 33-bus network) shows the characteristics of the approach and its feasibility for the analysis of real operating conditions.

The results show the significant impact of high aging failure probabilities on network reliability when the EV smart charging is absent, leading to increased power utility costs and customer losses. By adopting EV smart charging, the aging failure probabilities for cables and transformers are reduced by an average of 31% and 6%, respectively. Network reliability is improved, resulting in reduced node unavailability and EENS of 21 hours and 2.5 MWh, on average, respectively, for the 5-bus network. Likewise, the implementation of EV smart charging improves system reliability in the IEEE 33-bus network by reducing aging failure probabilities.

The most substantial improvement in network reliability is obtained by applying a smart charging strategy that minimalizes the total cost of customer loss and utilities (referred to as case 3 in this paper).

In this study, the clustered base load is adapted from historical data, as the principal focus is on the assessment of the capability of EV charging optimization to improve system reliability and reduce yearly customer costs. All the EVs are assumed as fully electric with the same charging power. However, accurate load prediction, incorporating EV load profile and considering additional factors (e.g., the combination of decentralized and centralized fast charging), deserves further investigation. Additionally, given the benefit of vehicle-to-grid technology, controlled discharging of EVs can be also integrated into the proposed reliability optimization model.

Restrictions on uncontrolled charging carry significant legal and economic implications, which have not been explicitly addressed in this paper. These aspects require specific consideration and further analysis to fully understand their impact on the implementation of EV charging policies.

REFERENCES

[1] R. C. Lotero and J. Contreras, "Distribution system planning with reliability," *IEEE Transactions on Power Delivery*, vol. 26, no. 4, pp. 2552-2562, Oct. 2011.

[2] J. Zhao, A. Arefi, and A. Borghetti, "End-of-life failure probability assessment considering electric vehicle integration," in *Proceedings of 2021 31st Australasian Universities Power Engineering Conference (AUPEC)*, Perth, Australia, Sept. 2021, pp. 1-6.

[3] S. Cheng, Z. Wei, D. Shang *et al.*, "Charging load prediction and distribution network reliability evaluation considering electric vehicles' spatial-temporal transfer randomness," *IEEE Access*, vol. 8, pp. 124084-124096, Jun. 2020.

[4] D. Božič and M. Pantoš, "Impact of electric-drive vehicles on power system reliability," *Energy*, vol. 83, pp. 511-520, Apr. 2015.

[5] M. R. Tur, "Reliability assessment of distribution power system when considering energy storage configuration technique," *IEEE Access*, vol. 8, pp. 77962-77971, Apr. 2020.

[6] M. Jooshaki, S. Karimi-Arpanahi, M. Lehtonen *et al.*, "Electricity distribution system switch optimization under incentive reliability scheme," *IEEE Access*, vol. 8, pp. 93455-93463, Apr. 2020.

[7] Z. Li, W. Wu, B. Zhang *et al.*, "Analytical reliability assessment method for complex distribution networks considering post-fault network reconfiguration," *IEEE Transactions on Power Systems*, vol. 35, no. 2, pp. 1457-1467, Mar. 2020.

[8] H. Shan, Y. Sun, W. Zhang *et al.*, "Reliability analysis of power distribution network based on PSO-DBN," *IEEE Access*, vol. 8, pp. 224884-224894, Jul. 2020.

[9] Q. Zhang, Y. Zhu, Z. Wang *et al.*, "Reliability assessment of distribution network and electric vehicle considering quasi-dynamic traffic flow and vehicle-to-grid," *IEEE Access*, vol. 7, pp. 131201-131213, Sept. 2019.

[10] H. Farzin, M. Fotuhi-Firuzabad, and M. Moeini-Aghtaie, "Reliability studies of modern distribution systems integrated with renewable generation and parking lots," *IEEE Transactions on Sustainable Energy*, vol. 8, no. 1, pp. 431-440, Jan. 2017.

[11] A. Hariri, M. A. Hejazi, and H. Hashemi-Dezaki, "Reliability optimization of smart grid based on optimal allocation of protective devices, distributed energy resources, and electric vehicle/plug-in hybrid electric vehicle charging stations," *Journal of Power Sources*, vol. 436, p. 226824, Oct. 2019.

[12] P. Srividhya, K. Mounika, S. Kirithikaa *et al.*, "Reliability improvement of radial distribution system by reconfiguration," *Advances in Science, Technology and Engineering Systems Journal*, vol. 5, no. 6, pp. 472-480, Nov. 2020.

[13] A. Noori, Y. Zhang, N. Nouri *et al.*, "Multi-objective optimal placement and sizing of distribution static compensator in radial distribution networks with variable residential, commercial and industrial demands considering reliability," *IEEE Access*, vol. 9, pp. 46911-46926, Mar. 2021.

[14] W. Sun, F. Neumann, and G. P. Harrison, "Robust scheduling of electric vehicle charging in LV distribution networks under uncertainty," *IEEE Transactions on Industry Applications*, vol. 56, no. 5, pp. 5785-5795, Mar. 2020.

[15] M. Naguib, W. A. Omran, and H. E. A. Talaat, "Performance enhancement of distribution systems via distribution network reconfiguration and distributed generator allocation considering uncertain environment," *Journal of Modern Power Systems and Clean Energy*, vol. 10, no. 3, pp. 647-655, Mar. 2022.

[16] C. A. P. Meneses and J. R. S. Mantovani, "Improving the grid operation and reliability cost of distribution systems with dispersed generation," *IEEE Transactions on Power Systems*, vol. 28, no. 3, pp. 2485-2496, Aug. 2013.

[17] X. Wang and R. Karki, "Exploiting PHEV to augment power system reliability," *IEEE Transactions on Smart Grid*, vol. 8, no. 5, pp. 2100-2108, Sept. 2017.

[18] O. Sadeghian, M. Nazari-Heris, M. Abapour *et al.*, "Improving reliability of distribution networks using plug-in electric vehicles and demand response," *Journal of Modern Power Systems and Clean Energy*, vol. 7, no. 5, pp. 1189-1199, Sept. 2019.

[19] A. Arefi, G. Ledwich, G. Nourbakhsh *et al.*, "A fast adequacy analysis for radial distribution networks considering reconfiguration and DGs," *IEEE Transactions on Smart Grid*, vol. 11, no. 5, pp. 3896-3909, Sept. 2020.

[20] A. Arefi, A. Abeygunawardana, and G. Ledwich, "A new risk-managed planning of electric distribution network incorporating customer engagement and temporary solutions," *IEEE Transactions on Sustain Energy*, vol. 7, no. 4, pp. 1646-1661, Oct. 2016.

[21] I. Ziari, G. Ledwich, S. Member *et al.*, "Integrated distribution systems planning to improve reliability under load growth," *IEEE Transactions on Power Delivery*, vol. 27, no. 2, pp. 757-765, Apr. 2012.

[22] M. P. Anand, B. Bagen, and A. Rajapakse, "Probabilistic reliability evaluation of distribution systems considering the spatial and temporal distribution of electric vehicles," *International Journal of Electrical Power and Energy Systems*, vol. 117, pp. 1-15, May 2020.

[23] Y. Li, K. Xie, L. Wang *et al.*, "The impact of PHEVs charging and

network topology optimization on bulk power system reliability," *Electric Power Systems Research*, vol. 163, pp. 85-97, Oct. 2018.
[24] M. D. Kamruzzaman and M. Benidris, "A reliability-constrained demand response-based method to increase the hosting capacity of power systems to electric vehicles," *International Journal of Electrical Power & Energy Systems*, vol. 121, pp. 1-11, Mar. 2020.
[25] M. D. Kamruzzaman and M. Benidris, "Reliability-based metrics to quantify the maximum permissible load demand of electric vehicles," *IEEE Transactions on Industry Applications*, vol. 55, no. 4, pp. 3365-3375, Jul.-Aug. 2019.
[26] K. Hou, X. Xu, H. Jia *et al*., "A reliability assessment approach for integrated transportation and electrical power systems incorporating electric vehicles," *IEEE Transactions on Smart Grid*, vol. 9, no. 1, pp. 88-100, Jan. 2018.
[27] A. N. Archana and T. Rajeev, "A novel reliability index based approach for EV charging station allocation in distribution system," *IEEE Transactions on Industry Applications*, vol. 57, no. 6, pp. 6385-6394, Nov.-Dec. 2021.
[28] M. S. Alam and S. A. Arefifar, "Optimal allocation of EV charging stations in distribution systems considering discharging economy and system reliability," in *Proceedings of IEEE International Conference on Electro Information Technology (EIT)*, Montana, USA, May 2021, pp. 355-362.
[29] S. Guner and A. Ozdemir, "Reliability improvement of distribution system considering EV parking lots," *Electric Power Systems Research*, vol. 185, pp. 1-11, Aug. 2020.
[30] W. Li, "Incorporating aging failures in power system reliability evaluation," *IEEE Transactions on Power Systems*, vol. 17, no. 3, pp. 918-923, Aug. 2002.
[31] J. Teh, C. M. Lai, and Y. H. Cheng, "Impact of the real-time thermal loading on the bulk electric system reliability," *IEEE Transactions on Reliability*, vol. 66, no. 4, pp. 1110-1119, Dec. 2017.
[32] A. Ahmadian, B. Mohammadi-Ivatloo, and A. Elkamel, "A review on plug-in electric vehicles: introduction, current status, and load modeling techniques," *Journal of Modern Power Systems and Clean Energy*, vol. 8, no. 3, pp. 412-425, May 2020.
[33] G. Parise, L. Martirano, L. Parise *et al.*, "A life loss tool for an optimal management in the operation of insulated LV power cables," *IEEE Transactions on Industry Application*, vol. 55, no. 1, pp. 167-173, Jan.-Feb. 2019.
[34] S. K. E. Awadallah, J. V. Milanovic, and P. N. Jarman, "The influence of modeling transformer age related failures on system reliability," *IEEE Transactions on Power Systems*, vol. 30, no. 2, pp. 970-979, Mar. 2015.
[35] C. F. Jekel and G. Venter. (2019, Mar.). PWLF: a Python library for fitting 1D continuous piecewise linear functions. [Online]. Available: https://github.com/cjekel/piecewise_linear_fit_py
[36] C. Huang, L. Cao, N. Peng *et al*., "Day-ahead forecasting of hourly photovoltaic power based on robust multilayer perception," *Sustainability (Switzerland)*, vol. 10, no. 12, pp. 4-11, Dec. 2018.
[37] Federal Highway Administration, U. S. Department of Transportation (2017, Dec.). National household travel survey. [Online]. Available: http://nhts.ornl.gov
[38] M. Farivar and S. H. Low, "Branch flow model: relaxations and convexification – Part I," *IEEE Transactions on Power Systems*, vol. 28, no. 3, pp. 2554-2564, Aug. 2013.
[39] S. H. Low, "Convex relaxation of optimal power flow – Part I: formulations and equivalence," *IEEE Transactions on Control Network Systems*, vol. 1, no. 1, pp. 15-27, Mar. 2014.
[40] J. M. Delarestaghi, A. Arefi, G. Ledwich *et al*., "A distribution network planning model considering neighborhood energy trading," *Electric Power Systems Research*, vol. 191, pp. 1-10, Feb. 2021.
[41] H. Turker, S. Bacha, D. Chatroux *et al*., "Low-voltage transformer loss-of-life assessments for a high penetration of plug-in hybrid electric vehicles (PHEVs)," *IEEE Transactions on Power Delivery*, vol. 27, no. 3, pp. 1323-1331, Jul. 2012.
[42] M. E. Baran and F. F. Wu, "Network reconfiguration in distribution systems for loss reduction and load balancing," *IEEE Transactions on Power Delivery*, vol. 4, no. 2, pp. 1401-1407, Apr. 1989.
[43] J. Zhao, A. Arefi, A. Borghetti *et al*., "Characterization of congestion in distribution network considering high penetration of PV generation and EVs," in *Proceesing of IEEE PES General Meeting (PESGM)*, Atlanta, USA, Aug. 2019, pp. 1–5.
[44] L. Lin, C. Chen, B. Wei *et al*., "Residential electricity load scenario prediction based on transferable flow generation model," *Journal of Electrical Engineering & Technology*, vol. 18, no. 1, pp. 99-109, Jan. 2023.
[45] A. Narimani, G. Nourbakhsh, A. Arefi *et al*., "SAIDI constrained economic planning and utilization of central storage in rural distribution networks," *IEEE System Journal*, vol. 13, no. 1, pp. 842-853, Mar. 2019.

Jinping Zhao received the B.S. and M.S. degrees in electrical engineering and automation from Lanzhou University of Technology, Lanzhou, China, in 2007 and 2011, respectively. She received the Ph.D. degree in electrical engineering from Murdoch University, Perth, Australia, in 2022. Currently, she is working as power systems engineer at Ingeteam Australia. Her research interests include power system planning, congestion management, and power quality.

Ali Arefi is an Associate Professor at the School of Engineering and Energy, Murdoch University, Perth, Australia. He has been the Chief Investigator in many national competitive grants with a total award of more than $11 million in research funds during 2016-2022, from which $4 million has been the research grants from the Government funders such as ARC Discovery Project, ARENA, Smart Cities and Suburbs Program, and the CRC Future Battery Institute and $7 million is from industry partners. In major funds, there have been extensive collaborations with industry partners in Australia. He has more than six years of experience in the electrical industry. He has been the consultant for 5 industry-funded research projects. Moreover, he has delivered many talks for industries in the field of energy efficiency and power quality. His research interests include sustainable electric distribution planning, state estimation, and energy efficiency.

Alberto Borghetti graduated in electrical engineering from the University of Bologna, Bologna, Italy, in 1992. Since then, he has been working with the power system group of the same university, where he is now a Professor of electrical power systems and resident corresponding member of the Academy of Sciences of the Bologna Institute. He received the 2018 CIGRE Technical Council Award for Study Committee C4. Currently, he is serving as an Associate Editor of Journal of Modern Power Systems and Clean Energy (MPCE). His research interests include power system analysis, lightning protection and electromagnetic transients, optimal generation scheduling, and distribution system operation.

Gerard Ledwich received the Ph.D. degree in electrical engineering from the University of Newcastle, Newcastle, Australia, in 1976. He is currently a Research Professor of electric power with the School of Electrical Engineering and Robotics, Queensland University of Technology, Brisbane, Australia. He has 215 journal publications and 323 refereed conference publications. He has a Scopus H-index of 44 and a citation count of 8633. He has been involved in securing grants of more than AU$16 million with the majority of them in explicit partnership with industry. His research interests include power systems, power electronics, and wide-area control of smart grid.